3D-Printed All-metal Wideband Dual-Polarization Cryogenic Dichroic Filters

Leif Helldner[1*], Denis Meledin[1], Saeed Khademzadeh[2], Yu Cao[2], Lars Nyborg[2], Igor Lapkin[1], Sven-Erik Ferm[1], Victor Belitsky[1], Alexey Pavolotsky[1], and Vincent Desmaris[1]

***Abstract*—In this work we report the performance of a 3D-printed single metallic layer high pass dichroic filter with an improved spectral response at non-normal beam incidence. The dichroic takes advantage of the extra degrees of freedom provided by metal additive manufacturing to enable the slanted design of the perforations of the dichroic metal plate. The dichroic demonstrates a good agreement between simulated and measured performance allowing transmission better than 90% and cross-polarization levels below -40 dB over a fractional bandwidth of about 28-30% in the Q-Band and could be scaled to higher THz frequency advantageously.**

***Keywords*—dichroic filters, mm-wave, additive manufacturing, metamaterial, 3D-printing.**

I. INTRODUCTION

DURING the last decade multiband receivers have gained significant attention in radio astronomy and environmental science [1-3]. Such receivers allow an improvement in the phase calibration for the higher frequency band, using the lower frequency band phase shift information due to the impact of atmospheric changes in the optical path. Moreover, faster mapping speed and enhanced UV-plane coverage make multiband receivers even more attractive, for example, to use in very large baseline interferometry (VLBI) observations. Frequency-selective surfaces (FSSs) commonly employed in multi-band receivers spatially divide a signal beam into two ones based on their difference in frequency. A dichroic filter, as a type of FSS, often employs a sequence of several patterned metallic and dielectric layers [4]. The geometrical properties such as the patterns' shapes and sizes, their periodicity, and the thickness of the metal and dielectric layers determine the frequency response of such dichroic.

The use of an all-metal design [5] offers the advantages of employing the dichroic filter at cryogenic temperatures, thereby minimizing system noise contributions through the improved metal conductivity and the reduced RF insertion loss, as well as reducing issues with outgassing and thermal contraction causing delamination.

In this work, we present a 3D-printed single-layer metallic dichroic filter for prospective reliable use at cryogenic temperatures. The filter allows the transmission of both polarization components of the input signal at a selected part of the Q-band (37-50 GHz), while reflecting the signal at the K-band (18-27 GHz), as it could be further used in a VLBI Tri-band receiver planned for Onsala Space Observatory (OSO) 20 m antenna. Yet, the design is perfectly scalable with an approach to explore additive manufacturing of a dichroic allowing transmission in other frequency bands.

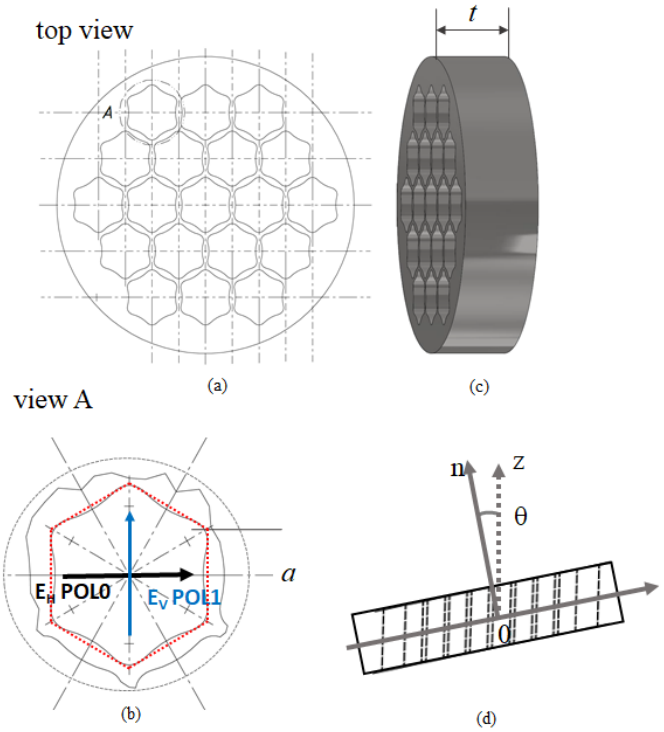

Fig. 1. The geometry of the designed perforated plate: (a) top view from *z* direction; (b) detailed top view A of the dichroic aperture from *z* direction; (c) and (d) - side view of the dichroic plate. The incident wave illuminates the dichroic plate with the angular offset of the apertures θ from the direction of z=∞. The side length of the initial hexagonal aperture is marked with a red color dot line.

II. DICHROIC DESIGN

The single-layer dichroic metal plate features perforations, as shown in Fig. 1, at a slant angle, θ, to minimize the angular degradation. The shape of the perforation has been first approximated using the equations in [5] and further optimized using HFSS simulations to reduce the insertion loss, eliminate in-band resonance spikes, and allow the transmission of both polarization of the input signal within the Q-band. A value of θ=13 degrees was considered acceptable for the proposed optical layout of the OSO Tri-band receiver, ensuring a fractional bandwidth of over 30%. Fig.2 shows the simulated transmission (TR) and cross-polarization characteristics (XPOL) as a function of frequency at 13 degrees of the waveguide aperture tilt, representing POL0 and POL1 polarizations, respectively. The incident radiation wave vector is always coaxial to the waveguide apertures. The transmission

[1]Group for Advanced Receiver Development, Department of Space, Earth and Environmental Sciences, Chalmers University of Technology, Gothenburg, SE-41296, Sweden; [2]Materials and manufacture, Department of industrial and Materials Science, Chalmers University of Technology, Gothenburg, SE-41296, Sweden. *Corresponding author (email: leif.helldner@chalmers.se).

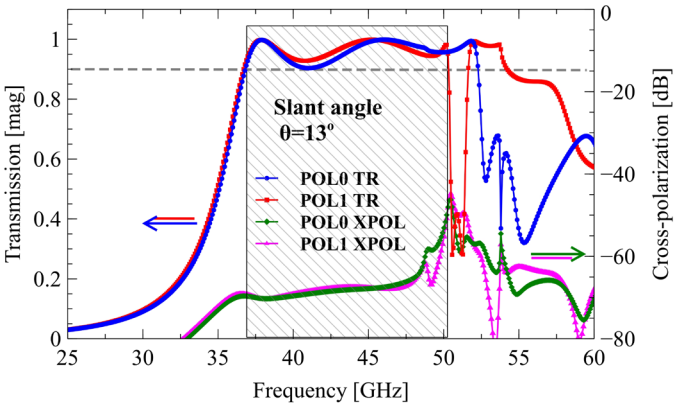

Fig. 2. Simulated transmission (TR, left axis) for horizontally (E_H) oriented E–field (POL0) and vertically (E_V) oriented E–field (POL1), and cross-polarization characteristics (XPOL, right axis) between the polarizations of the designed dichroic filter as a function of the frequency at the designed value of slant angle θ=13 degrees. The frequency ranges with transmission exceeding 90% are indicated by the hatched areas. This transmission level is indicated by a gray dashed line.

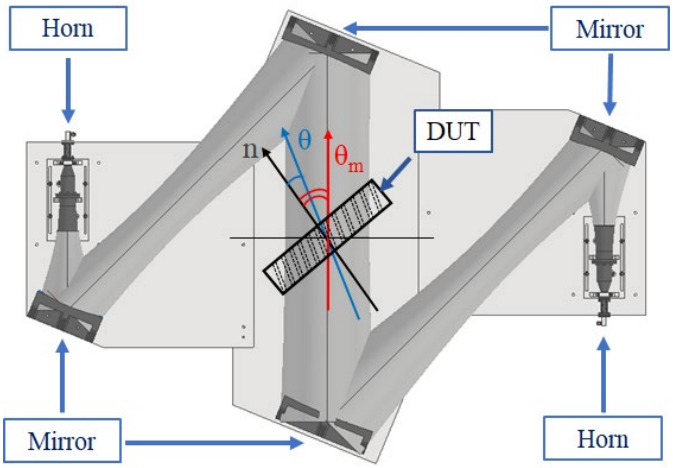

Fig. 4. The schematic layout of the optical assembly for the characterizing the dichroic filter, the grey-shaded volume represents the calculated quasi-optical beam indicating the path of the beam within the system; A photograph of the measurement setup can be seen in [5]

for frequencies lower than 27 GHz is expected to be below 5%. The cross-polarization simulations show a negligible effect on the performances, consistently staying well below the threshold value of -40 dB.

III. DICHROIC FABRICATION

The dichroic has been fabricated using additive manufacturing to enable the electromagnetic design of the dichroic with slanted perforations. For this study, gas-atomized $Al_{10}SiMg$ powder was selected as the starting material. The prototype was fabricated using the Powder Bed Fusion Laser Beam (PBF-LB) additive manufacturing process in an EOS M290 machine with a 100 µm spot size and a 400 W (370 W nominal power) Yb-fiber laser. Optimum precision process parameters were used to achieve the maximum density and minimum deviation from the predesigned model.

Prior to cutting the printed part from the build plate, stress relief heat treatment was conducted at 300°C for 3 hours, followed by furnace cooling. The printed dichroic plate was then cut from the platform using a cold saw. To inhibit the deformation of thin walls in honeycomb structures during cutting, the voids were filled with hard wax. To achieve further dimensional accuracy, the bottom of the dichroic plate was then surface-finished in a precision milling machine, followed by wax removal.

The manufactured dichroic filter prototype is 7.11 mm thick and its features are shown in Fig. 3.

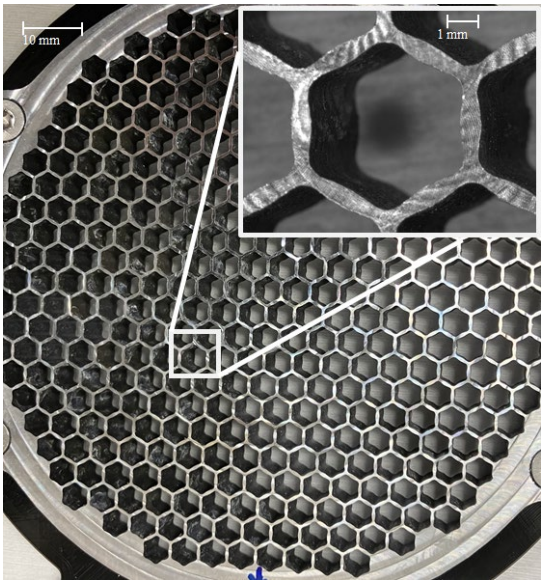

Fig. 3. Manufactured dichroic filter. The insert provides a close-up view of a single perforation cell, highlighting the details of its structure. The view is taken from the *n*-direction (see Fig. 1).

IV. DICHROIC CHARACTERISATION AND PERFORMANCE

The electromagnetic performance of the 3D-printed dichroic was obtained using a Vector network analyzer coupled to a quasi-optical system that provides a plane-wave-like beam at the position where the tested dichroic is installed. The setup consists of four ellipsoidal mirrors with horn antennas at the transmitting and receiving sides. The layout of the measurement setup, visualizing the propagated beams, is illustrated in Fig. 4. To prevent any parasitic reflections, the area outside of 4 times the beam at the dichroic plate is shielded with an absorber. Moreover, polarization grids have been incorporated into the optical system to minimize cross-polarization levels. The waveguide aperture tilt θ=13degrees is indicated in Fig. 4 with a blue arrow, the incident angle θ_m represents the apparent angle between the beam axis, indicated by a red arrow, and the normal direction to the metal plate *n*, marked with a dark grey arrow.

The comparison between simulated and measurement transmission as well as cross-polarization characteristics was carried out for POL1 as depicted in Fig.5a. It is evident from the figures that the measurement results closely align with the simulated transmission data exhibiting a fractional bandwidth of about 30%. The measured low edges of the filter (defined as 90% transmission) passband match well with simulations with

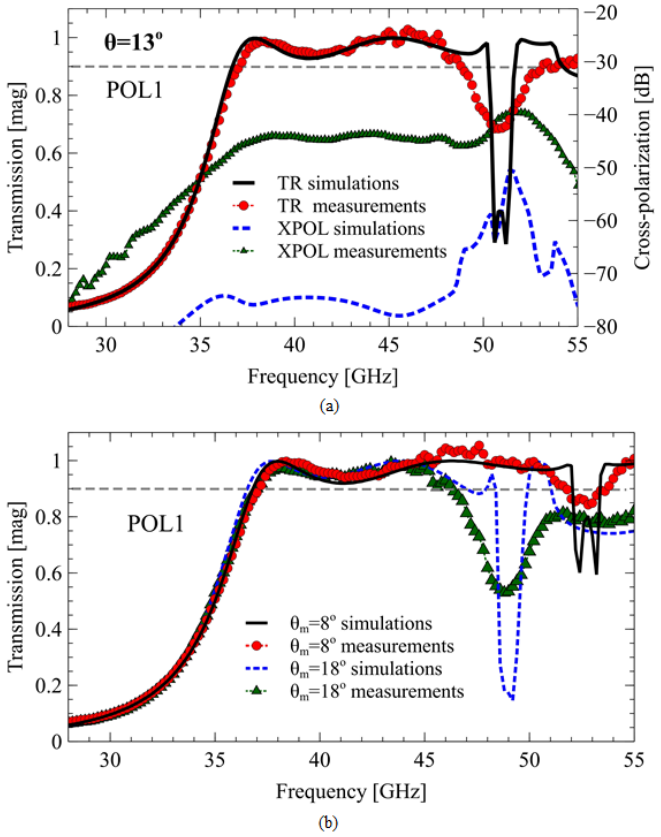

Fig. 5. The comparison between simulated and measurement transmission as well as cross-polarization characteristics for POL1: a.) transmission (TR, left axis), and cross-polarization characteristics (XPOL, right axis) between polarizations of the designed dichroic filter as a function of the frequency at the designed value of slant angle θ=13 degrees. b.) transmission at $\Delta\theta$=±5 degrees: A transmission level of 90% is indicated by gray dashed lines.

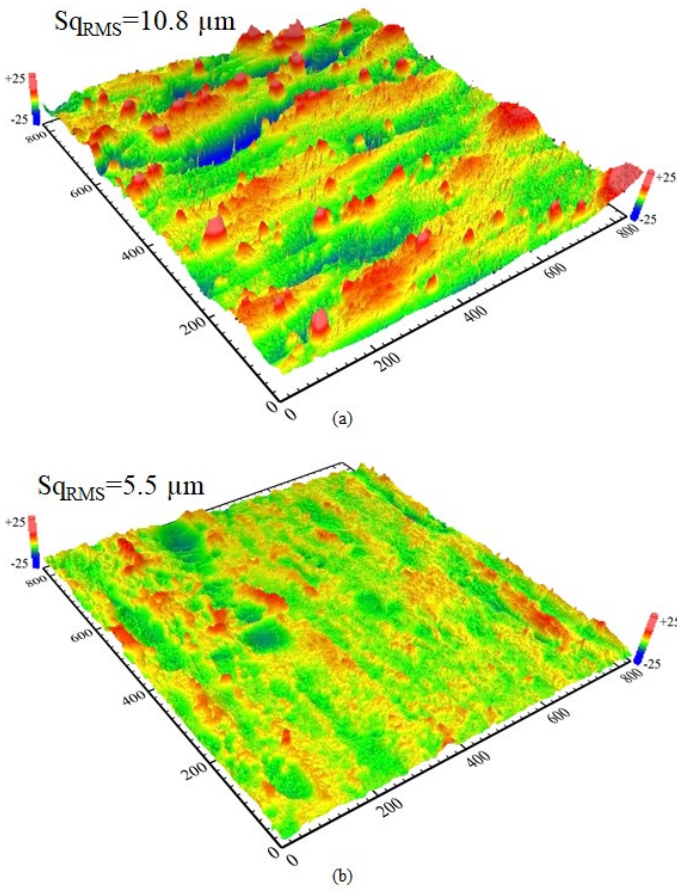

Fig. 6. The 3D surface scan of a). the 3D-printed dichroic filter presented in this work; b), Laser milled fabricated dichroic filter presented in [5]

an accuracy of about 0.2 GHz. The measured cross-polarization leakage remains better than 40 dB across the entire passband for both polarizations, fully satisfying the practical design requirements. For the cross-polarization plots in Fig.5a, the only case represented is when POL1 was excited and POL0 was detected.

In order to verify the accuracy of our model, we performed the measurements of the fabricated dichroic with a manufactured aperture tilt of θ =13 degrees at different values of $\theta_m=\theta\pm\Delta\theta$, where $\Delta\theta$ was set to ±5 degrees (see Fig.4). In the HFSS simulations, the angle θ was kept always at 13 degrees and $\Delta\theta$ values were an angle between the waveguide walls axis and the incident wave axis. In Fig.5b we depict a comparison between the measured transmission and the corresponding simulated values for POL1 at $\Delta\theta$ = ±5 degrees, respectively. The simulated transmission closely matched the measured results at both values of θ_m varied in the experiments. The measurement results prove the feasibility of the dichroic filter design with desirable frequency and polarization performance.

It is important to acknowledge that our simulations did not take into account the roughness of the metal plate surface and the perforation walls. However, we compared surface quality between the 3D printed dichroic presented in this work and the laser-cut dichroic filter with tilted perforations for the Q-band reported in [5]. Measured RMS surface roughness (Sq_{RMS}) values presented in Fig.6 for both devices demonstrate surface roughness of the same order of magnitude (relative to the skin depth on such material at mm-wave frequencies) for the 3D printed dichroic and the other filter fabricated employing laser cutting technology. Therefore, despite the difference in surface roughness values, both dichroic filters demonstrate very similar performances allowing fractional bandwidth of about 30% with transmission better than 90% and exceptional cross-polarization levels below -32 dB.

V. CONCLUSION

We have proposed a design for the dichroic filter based on a perforated metal plate fabricated using 3D printing with additive manufacturing. The proposed design can reach 90% of the transmission about 30% of the RF bandwidth around 43 GHz central frequency. The measured performance showed a very good agreement with the simulations. The presented design is scaleable to higher frequencies and could be employed as a cold dichroic filter for providing simultaneous operation at higher frequencies, for instance, e.g. 230 and 345 GHz channels of the Event Horizon Telescope. Despite a difference in surface roughness between the 3D-printed dichroic fabricated by additive manufacturing and the one manufactured using water-guided laser cutting, both dichroic filters show very similar performances in the Q-band frequency range. Thereby shows that 3D metal printing is very suitable for producing advanced

mm-wave dichroic and opens up for novel and more advanced designs of components in the mm-wave frequency range.

REFERENCES

[1] M. Carter, et al., "The EMIR multi-band mm-wave receiver for the IRAM 30-m telescope," *Astron. Astrophys.*, vol. 538, Art. no. A89, February 2012, Available: DOI: 10.1051/0004-6361/201118452. [Accessed: June. 24, 2024].

[2] S.-T. Han, et al., "Korean VLBI network receiver optics for simultaneous multifrequency observation: Evaluation," *Pub. Astron. Soc. Pac.*, vol. 125, no. 927, p. 539, May 2013. Available: DOI: 10.1086/671125. [Accessed: June. 24, 2024].

[3] N. Okada, et al., "Development of the multi-band simultaneous observation system of the Nobeyama 45-m Telescope in HINOTORI (Hybrid Installation project in NObeyama, Triple-band ORIented)", *Proceedings of the SPIE*, vol.11453, art. id. 1145349, December 2020. Available: DOI: 10.1117/12.2562137. [Accessed: June. 27, 2024].

[4] X. You, C. Fumeaux and W. Withayachumnankul, "Tutorial on broadband transmissive metasurfaces for wavefront and polarization control of terahertz waves", *J. Appl. Phys.,* vol. 131, art. id 061101, February 2022. Available: DOI: doi.org/10.1063/5.0077652. [Accessed: June. 27, 2024].

[5] D. Montofré, et al., "A Broad-Band Dual-Polarization All-Metal Dichroic Filter for Cryogenic Applications in Sub-THz Range," *IEEE Transactions on Terahertz Science and Technology*, vol. 14, no.2, p. 199, March 2024. Available: DOI: 10.1109/TTHZ.2023.3338472 [Accessed: June. 17, 2024].